Effect of chemical reactions on decaying isotropic turbulence

M. Pino Martín and Graham V. Candler
*Department of Aerospace Engineering and Mechanics, University of Minnesota, 110 Union St. SE,
Minneapolis, Minnesota 55455*

There have been many studies of turbulent combustion flows, however the interaction between turbulent motion and the chemical reactions that occur in hypersonic flows has not been studied. In these flows, the rate of product formation depends almost exclusively on the temperature, and small temperature fluctuations may produce large changes in the rate of product formation. To study this process, we perform direct numerical simulations of reacting isotropic turbulence decay under conditions typical of a hypersonic turbulent boundary layer flow. We find that there is a positive feedback between the turbulence and exothermic reactions. That is, positive temperature fluctuations increase the reaction rate, thereby increasing the heat released by the reaction, which further increases the temperature. Simultaneously, the pressure increases causing localized expansions and compressions that feed the turbulent kinetic energy. The Reynolds stress budget shows that the feedback occurs through the pressure-strain term. We also find that the strength of the feedback depends on how much heat is released, the rate at which it is released, and the turbulent Mach number. The feedback process is negative for endothermic reactions, and temperature fluctuations are damped. © *1998 American Institute of Physics.* [S1070-6631(98)00307-9]

I. INTRODUCTION

The interaction between turbulent fluid motion and finite-rate chemical reactions has not been studied under conditions typical of a high-temperature, hypersonic boundary layer. These flows are significantly different than turbulent combustion flows, which have been studied extensively. In hypersonic flows the dominant chemical reactions are the dissociation and recombination of nitrogen and oxygen molecules. These reactions are different than combustion reactions for several reasons. First, the equilibrium composition of reacting air depends strongly on the temperature. This is contrasted with a combustion process, where the equilibrium composition is determined by the initial fuel-oxidizer ratio. Another important feature of air reactions is that they have a large activation energy, and therefore the reaction rate is typically temperature limited. In this situation, the reaction rate depends exponentially on the temperature, and small increases in the temperature result in large increases in the reaction rate. This is contrasted with non-premixed combustion flows where the fuel-oxidizer mixing rate determines the rate of product formation, and the reaction process is relatively insensitive to the temperature. In premixed combustion flows, the flame speed is primarily determined by the diffusive transport of reactive radical species and heat, rather than by the reaction rate itself.[1]

The surface of a hypersonic vehicle is typically cooled below the adiabatic wall temperature. Thus, the maximum temperature in a hypersonic boundary layer occurs some distance from the surface where there is significant shear heating and the wall cooling is not important. In this region, the air molecules dissociate, and the reaction products diffuse toward the surface where they recombine due to the cool wall. Therefore, hypersonic boundary layers, unlike combus-

tion flows, have regions of endothermic (dissociation) reactions and exothermic (recombination) reactions.

Thus, it is the purpose of this paper to study how turbulent temperature fluctuations interact with the finite-rate chemical reactions that occur in hypersonic boundary layers. We numerically solve the compressible Navier–Stokes equations that have been extended to include the effects of finite-rate chemical reactions and heat release. We study how changes in the reaction rate, heat release, and turbulent Mach number affect the decay of isotropic, homogeneous turbulence. Isotropic turbulence is the most fundamental turbulent flow, and it is a useful idealized test case. It also serves as an approximation of the small-scale turbulent motion in a boundary layer.

Many direct numerical simulations of reacting turbulent flows have been reported for combustion applications.[2–14] However, as mentioned above, these simulations focus on different issues than the current paper. For example, Gao and O'Brien[6] and Javery *et al.*[14] consider the interaction of chemical reactions with homogeneous turbulence, but the reaction rate is taken as constant and the effects of heat release are not considered. Picart *et al.*[3] consider a concentration-dependent reaction rate to simulate the exponential dependence of the reaction rate on temperature, but their simulations do not include heat release effects. Several simulations of reacting shear layers have been performed including the effects of heat release. McMurtry *et al.*[5] and Grinstein and Kailasanath[8] use a constant reaction rate, and Givi *et al.*[7] and Miller *et al.*,[10] consider both constant and temperature-dependent reaction rates. These simulations show a significant effect of heat release on the structure of the mixing layers studied. Therefore, the previous simulations have

1715

some similarity to those presented here, but they focus on different, combustion-related issues.

In the remainder of the paper, we introduce the equations of motion and relevant non-dimensional parameters for a mixture of reacting gases. We then discuss the formulation of our direct numerical simulations and present the results. Finally, we analyze the chemistry–turbulence interaction process and summarize our findings.

II. GOVERNING EQUATIONS

The equations describing the unsteady motion of a reacting flow with no contribution of vibrational modes are given by the species mass, mass-averaged momentum, and total energy conservation equations

$$
\frac{\partial \rho_s}{\partial t} + \frac{\partial}{\partial x_j}(\rho_s u_j + \rho_s v_{sj}) = w_s,
$$

$$
\frac{\partial \rho u_i}{\partial t} + \frac{\partial}{\partial x_j}(\rho u_i u_j + p\,\delta_{ij} - \tau_{ij}) = 0, \tag{1}
$$

$$
\frac{\partial E}{\partial t} + \frac{\partial}{\partial x_j}\left((E+p)u_j - u_i\tau_{ij} + q_j + \sum_s \rho_s v_{sj} h_s\right) = 0,
$$

where w_s represents the rate of production of species s due to chemical reactions; ρ_s is the density of species s; u_j is the mass-averaged velocity in the j direction; v_{sj} is the diffusion velocity of species s; p is the pressure; τ_{ij} is the shear stress tensor given by a linear stress-strain relationship; q_j is the heat flux due to temperature gradients; h_s is the specific enthalpy of species s; and E is the total energy per unit volume given by

$$
E = \sum_s \rho_s c_{vs} T + \frac{1}{2}\rho u_i u_i + \sum_s \rho_s h_s^\circ, \tag{2}
$$

where c_{vs} is the specific heat at constant volume of species s; and h_s° represents the heat of formation of species s.

To derive the expression for w_s, consider a reaction where species S1 reacts to form species S2

$$
\text{S1} + \text{M} \rightleftharpoons \text{S2} + \text{M}, \tag{3}
$$
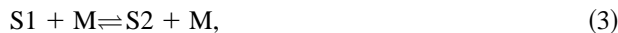
where M represents a collision partner, which is either S1 or S2 in this case. The source terms for S1 and S2 can be written using the law of mass action

$$
w_{S1} = -M_{S1}k_f \frac{\rho_{S1}}{M_{S1}}\left(\frac{\rho_{S1}}{M_{S1}} + \frac{\rho_{S2}}{M_{S2}}\right)
$$

$$
+ M_{S1}k_b \frac{\rho_{S2}}{M_{S2}}\left(\frac{\rho_{S1}}{M_{S1}} + \frac{\rho_{S2}}{M_{S2}}\right), \tag{4}
$$

and $w_{S2} = -w_{S1}$; k_f and k_b are the forward and backward reaction rates respectively. These are written as

$$
k_f = C_f\, T^\eta\, e^{-\theta/T}, \qquad k_b = \frac{k_f}{K_{eq}}, \tag{5}
$$

where K_{eq} is the temperature-dependent equilibrium constant.

For a two species mixture, the diffusion velocity can be accurately represented using Fick's law

$$
\rho_s v_{sj} = -\rho D \frac{\partial c_s}{\partial x_j}, \tag{6}
$$

where $c_s = \rho_s/\rho$ is the mass fraction, and D is the diffusion coefficient given in terms of the Lewis number

$$
\text{Le} = \frac{\rho D \text{Pr}}{\mu}, \tag{7}
$$

where Pr is the Prandtl number, μ is the viscosity, and Le is taken to be unity, so that the energy transport due to mass diffusion is equal to the energy transport due to thermal conduction.

III. GOVERNING PARAMETERS

In this section, we introduce the nondimensional numbers governing the physical process. From a nondimensional analysis of the governing equations, the following parameters are obtained: turbulent Mach number, M_t; Reynolds number based on the Taylor microscale, Re_λ; Damköhler number, Da; and relative heat release, $\overline{\Delta h^\circ}$. The turbulent state of the flow gives rise to the first two nondimensional numbers; the second two are present if the flow is chemically reacting. These parameters may be written as

$$
M_t = \frac{q}{a}, \qquad Re_\lambda = \frac{\rho u'\lambda}{\mu},
$$

$$
\text{Da} = \frac{\lambda|w|}{\rho u'}, \qquad \overline{\Delta h^\circ} = -\frac{\Delta h^\circ}{c_v T + \frac{1}{2}q^2}, \tag{8}
$$

where q is the rms magnitude of the fluctuation velocity; a is the speed of sound; u' is the rms turbulent velocity fluctuation in one direction; $\Delta h^\circ = h_{S2}^\circ - h_{S1}^\circ$ is the heat of the reaction; and c_v is the mixture specific heat at constant volume.

The Damköhler number is the ratio of the turbulent time scale, τ_t, to the chemical time scale, τ_c, and represents a nondimensional reaction rate; here $\tau_t = \lambda/u'$ and $\tau_c = \rho/|w|$. $\overline{\Delta h^\circ}$ is the ratio of the chemical energy released or absorbed to the sum of the internal and kinetic energy. A negative value indicates an endothermic reaction, and a positive value denotes an exothermic reaction.

IV. NUMERICAL EXPERIMENTS

It is the purpose of this paper to determine how turbulent motion interacts with the chemical reactions that occur in hypersonic boundary layers. A logical reaction to consider is the dissociation and recombination of nitrogen, $N_2 + M \rightleftharpoons 2N + M$. However, we have found that it is difficult to analyze the effects of this reaction on the decay of isotropic turbulence because many parameters change simultaneously during the reaction. For example, consider a case where we start with pure nitrogen atoms, and let them recombine according to the reaction rate and equilibrium constant expressions given by Gupta et al.[15] Figure 1 plots the nitrogen molecule mass fraction for simulations with initial temperatures between 2000 and 7000 K (corresponding to values of relative heat release between 33 and 9). We see that the equilibrium mass fraction depends on the initial temperature be-
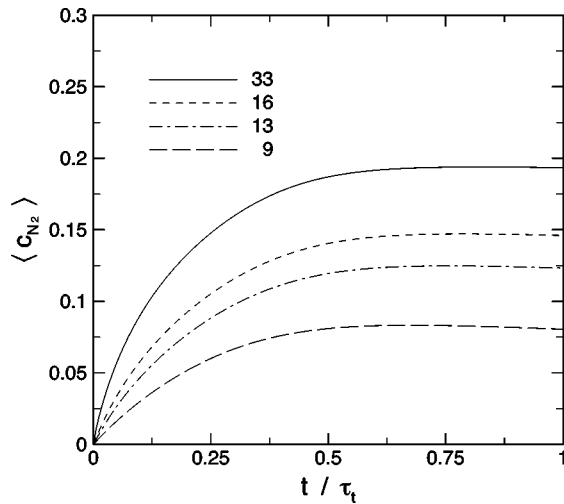
FIG. 1. Time evolution of the average N_2 mass fraction for simulations of recombining nitrogen atoms at initial $M_t = 0.519$, $Re_\lambda = 34.5$, and $\overline{\Delta h°} = 33$, 16, 13, and 9, corresponding to initial $T_o = 2000$, 4000, 5000, and 7000 K, respectively.

cause the equilibrium constant is a function of temperature. More importantly, the rate of reaction differs in each simulation. The differences between the simulations make it difficult to compare the effects of turbulent motion on the evolution of the chemical reactions. Therefore, we must devise a simplified chemical model that captures the key features of air reactions, yet makes it possible to compare simulations.

There are several issues that we must consider. First, if the average molecular weight of the gas changes when the reaction occurs, then the mixture-averaged gas constant and specific heats change. Therefore, changes in the pressure and internal energy will not only be due to the heat released by the reaction, but also due to the changing properties of the gas mixture. To circumvent this issue, we let the reactant and product have the same molecular weight and the same number of internal degrees of freedom; thus the mixture gas constant and specific heats do not change as the reaction progresses. For the same reason, we use the simple binary reaction given in (3), rather than a dissociation reaction in which the average molecular weight of the gas changes as a result of the reaction.

As discussed above, the equilibrium constant is a function of temperature, which implies a different chemical equilibrium state for simulations with different heat release. Therefore, we take K_{eq} to be constant, so that the equilibrium chemical state is fixed. This allows us to systematically compare simulations with different initial conditions and values of heat release.

The reaction rate is also a function of temperature. When the temperature increases the reaction rate grows exponentially, which presents similar problems with comparing one simulation to another. Therefore, we must modify the Arrhenius form of the reaction rate given by (5). It is desirable that the modified reaction rate be constant when there are no temperature fluctuations, and that the rate vary exponentially when there are temperature fluctuations. One such reaction rate expression is given by

$$\tilde{k}_f(T) = C \frac{e^{-\theta/T}}{e^{-\theta/\langle T \rangle}},$$

$$= C \left(1 + \frac{\theta}{\langle T \rangle} \frac{T'}{T} + \frac{1}{2} \left(\frac{\theta}{\langle T \rangle} \frac{T'}{T} \right)^2 + \dots \right), \tag{9}$$

where $\langle T \rangle$ is the ensemble average of the temperature, $T' = T - \langle T \rangle$ is the temperature fluctuation, C is a constant, and θ is the activation temperature given in (5). If for both reaction rate expressions we compute the ratio of the reaction rate at temperature T, to that at the ensemble-average temperature, $\langle T \rangle$, we obtain

$$\frac{k_f(T)}{k_f(\langle T \rangle)} = \frac{\tilde{k}_f(T)}{\tilde{k}_f(\langle T \rangle)} = e^{-(\theta/T - \theta/\langle T \rangle)}. \tag{10}$$

Note that we have neglected the preexponential factor in the reaction rate, T^η, because for the reactions that occur in hypersonic flows, $\eta \lesssim -1$. Thus, at large temperatures, this factor has a weak, sublinear variation with temperature. Therefore, the two rate expressions give the same variation of the relative reaction rate for any temperature fluctuation. The only difference is that the modified reaction rate expression gives a constant rate when the temperature is equal to the ensemble-average temperature. Thus, the modified reaction rate has the important features of the Arrhenius rate expression, yet allows us to systematically compare simulations.

V. NUMERICAL METHOD AND INITIAL CONDITIONS

In this section we present the numerical simulations for three-dimensional, compressible, homogeneous, isotropic, reacting turbulent flow. The numerical method used is based on the method of Lee et al.[16] We use a sixth-order accurate finite-difference method based on a compact Padé scheme and fourth-order accurate Runge–Kutta time integration. The simulations were performed on grids with 96^3 points following the criteria given by Reynolds[17] and a resolution of $K\eta = 1$ at the end of the simulation, where K is the maximum wavenumber resolvable on the grid and η is the Kolmogorov scale. The computational domain is a periodic box with nondimensional length 2π in each direction. The velocity field is initialized to an isotropic state prescribed by the following energy spectrum,

$$E(k) \sim k^4 \exp \left[-2 \left(\frac{k}{k_o} \right)^2 \right], \tag{11}$$

where k is the integer nondimensional wavenumber, and k_o is the most energetic wavenumber.

As Ristorcelli and Blaisdell[18] show, in a physically consistent initialization of compressible homogeneous, isotropic turbulence, there are finite density, temperature, and dilatational fluctuations. Therefore, we use their initial conditions and have compared and validated our flow initialization with that of Blaisdell and Ristorcelli.[19]

We let the turbulence evolve to a realistic state before allowing the reaction to progress. Because the initial field is weakly compressible, we use mean values of velocity derivative skewness, S_i, to predict the onset of realistic turbulence. Experimental data presented by Tavoularis et al.[20] and

Orszag *et al.*[21] show that S_i is in the range $[-0.6: -0.35]$ for Re_λ near 50. With this criterion, the turbulence has developed to a realistic, isotropic state at $t/\tau_t = 0.35$. The reaction is started at this time, and we measure the evolution of the turbulence relative to this time.

We run cases with combinations of $\overline{\Delta h^\circ} = -0.5$, 1.0, 1.5, and 2.0; Da=0.5, 1.0, and 2.0; $M_t = 0.173$, 0.346, and 0.519; and $Re_\lambda = 25.0$, 34.5, and 50.0. We use nitrogen atoms for both species S1 and S2, with initial mass fractions of $c_{S1} = 1$ and $c_{S2} = 0$. We choose $K_{eq} = 1$, so that the chemical equilibrium is reached when $c_{S1} = c_{S2} = 0.5$. k_o is set to 4. To simplify the comparison of different simulations, we freeze μ at its initial value, and we use Pr=0.72. We specify the initial density as $\rho_o = 1.0$ kg/m^3. To be consistent with the physical N$_2$ dissociation rate, we use $\theta = 113,200$ K.

Having introduced the modified reaction rate (9), we must specify an initial temperature that is representative of a hypersonic boundary layer and consistent with the physically correct reaction rate (5). Using the law of mass action given by (4) and assuming that we initialize the flow with pure S1, we can obtain an expression for the initial source term and combine it with (8) to derive the initial rate of reaction

$$k_f = \frac{1}{3} \frac{\gamma \, M_t^2 \, \text{Da} \, \hat{R} \, T_{ref}^n}{\mu_{ref} \, Re_\lambda} \, T^{1-n}, \tag{12}$$

where we have taken μ from a power law $[\mu = \mu_{ref}(T/T_{ref})^n]$, μ_{ref} from a Sutherland law,[15] and $\hat{R}$ is the universal gas constant. In order to obtain realistic conditions, we choose the parameters in the modified reaction rate expression, (9), to be representative of the nitrogen dissociation reaction. To do so, we use the N$_2$ dissociation rate expression[15]

$$k_f = 3.71 \times 10^{21} \, T^{-1.6} \, e^{-113,200/T} \quad (\text{cm}^3/\text{mole s}). \tag{13}$$

We then set this expression equal to the reaction rate in terms of the nondimensional parameters, (12), and find the temperature that satisfies this relation. For $M_t = 0.3$, Da=0.5, $T_{ref} = 300$ K, $Re_\lambda = 50$, and $\mu_{ref} = 2.106 \times 10^{-4}$ kg/m s, and nitrogen ($n = 0.7722$), we obtain an initial value of $T = 9470$ K. This initial temperature is characteristic of a high-temperature hypersonic boundary layer.

VI. RESULTS

We first focus on how the chemical reactions affect the gas dynamics, leaving the discussion of the chemistry and turbulence interaction for the next section. During a typical reacting simulation, the average concentration of species S1 decreases as the average concentration of species S2 increases. It should be noted that as the chemical species reach the equilibrium mass fraction, $c_{S1} = c_{S2} = 0.5$, the rate at which energy is added to or removed from the fluid approaches zero.

A. Relative heat release

In this section, we illustrate the effect of variations of the relative heat release at moderate Da, M_t, and Re_λ (Da=1, $M_t = 0.346$, and $Re_\lambda = 34.5$). In all cases the nonreacting simulation is shown for comparison purposes. As mentioned
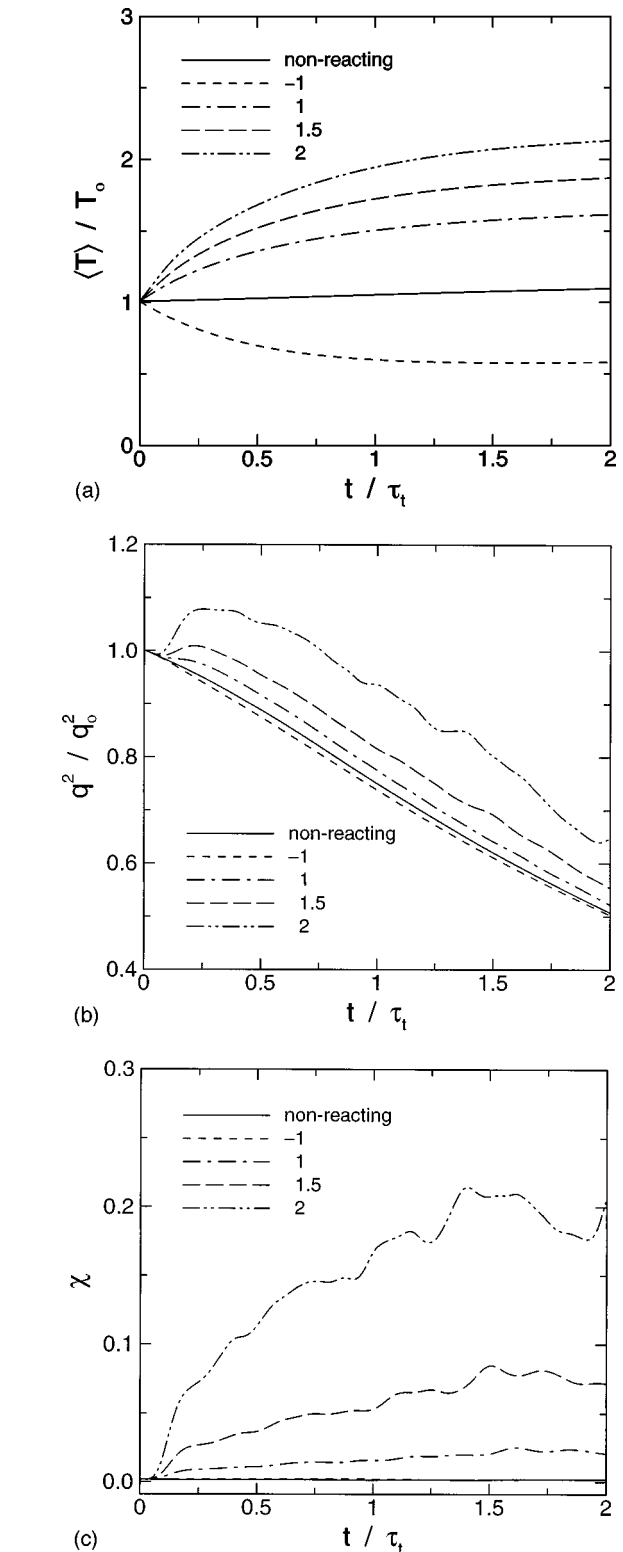

FIG. 2. Time evolution of (a) average temperature; (b) turbulent kinetic energy; and (c) relative compressible kinetic energy showing the effect of $\overline{\Delta h^\circ}$ for Da=1, $M_t = 0.346$, and $Re_\lambda = 34.5$.

earlier, the relative heat release is proportional to the ratio of energy released or absorbed in the formation of product species. Therefore, an increase in $\overline{\Delta h^\circ}$ increases the energy in the flow field. This is illustrated in Fig. 2(a), which plots the

temporal evolution of the average temperature. Figure 2(b) shows the temporal evolution of the turbulent kinetic energy for the different values of $\overline{\Delta h^\circ}$. When $\overline{\Delta h^\circ} = 1$, there is an initial period of time when the turbulence is enhanced. A further increase of the heat release considerably enhances the turbulent kinetic energy, maintaining and feeding the turbulence for a longer period of time.

Turbulent motion is dissipative, and needs a supply of energy to keep from decaying. Moyal[22] decomposed the velocity field in Fourier space, $\hat{\mathbf{u}}$, into the incompressible (divergence-free), $\hat{\mathbf{u}}^I$, and compressible (curl-free), $\hat{\mathbf{u}}^C$, components

$$\hat{\mathbf{u}}^I = \hat{\mathbf{u}} - \frac{\mathbf{k} \cdot \hat{\mathbf{u}}}{k^2} \mathbf{k},$$

$$\hat{\mathbf{u}}^C = \hat{\mathbf{u}} - \hat{\mathbf{u}}^I. \tag{14}$$

The dissipation for isotropic turbulence can then be written as

$$\epsilon = 8 \pi \nu \int_0^\infty \left(E^I(k) + \frac{4}{3} E^C(k) \right) k^2 \, dk, \tag{15}$$

where E^I and E^C represent the incompressible and compressible components of the shell-averaged energy spectrum

$$E^C = \frac{\hat{\mathbf{u}}^C \cdot \hat{\mathbf{u}}^C}{2 k},$$

$$E^I = \frac{\hat{\mathbf{u}}^I \cdot \hat{\mathbf{u}}^I}{2 k}. \tag{16}$$

From (15) we see that as the compressibility of the flow increases, the turbulence becomes more dissipative. This explains the increased rate of turbulent kinetic energy decay for the higher heat release flows.

Figure 2(c) shows the evolution of the relative compressible energy ratio

$$\chi = \frac{\int E^C(k) \, dk}{\int (E^C(k) + E^I(k)) \, dk}. \tag{17}$$

Because the simulations begin with weakly compressible conditions, when the turbulence reaches a realistic state, the initial values of χ are very low. For the endothermic reaction, χ is very small throughout the simulation, and as $\overline{\Delta h^\circ}$ is increased, the relative compressible kinetic energy increases. For a relative heat release of $\overline{\Delta h^\circ} = 2$, χ increases rapidly and E^C reaches about 20% of the total kinetic energy at $t/\tau_t = 1.3$. Also note that there are time-dependent oscillations in χ that increase with the heat release.

Consider the energy spectrum of the flow field decomposed into its incompressible and compressible components at several different times during the simulations. Figure 3(a) plots these spectra for the nonreacting simulation. We observe that the compressible modes are about two orders of magnitude less energetic than the incompressible modes at all but the smallest scales. However, note that for $k \eta > 1$, the length scales are not resolved by the simulation; thus the
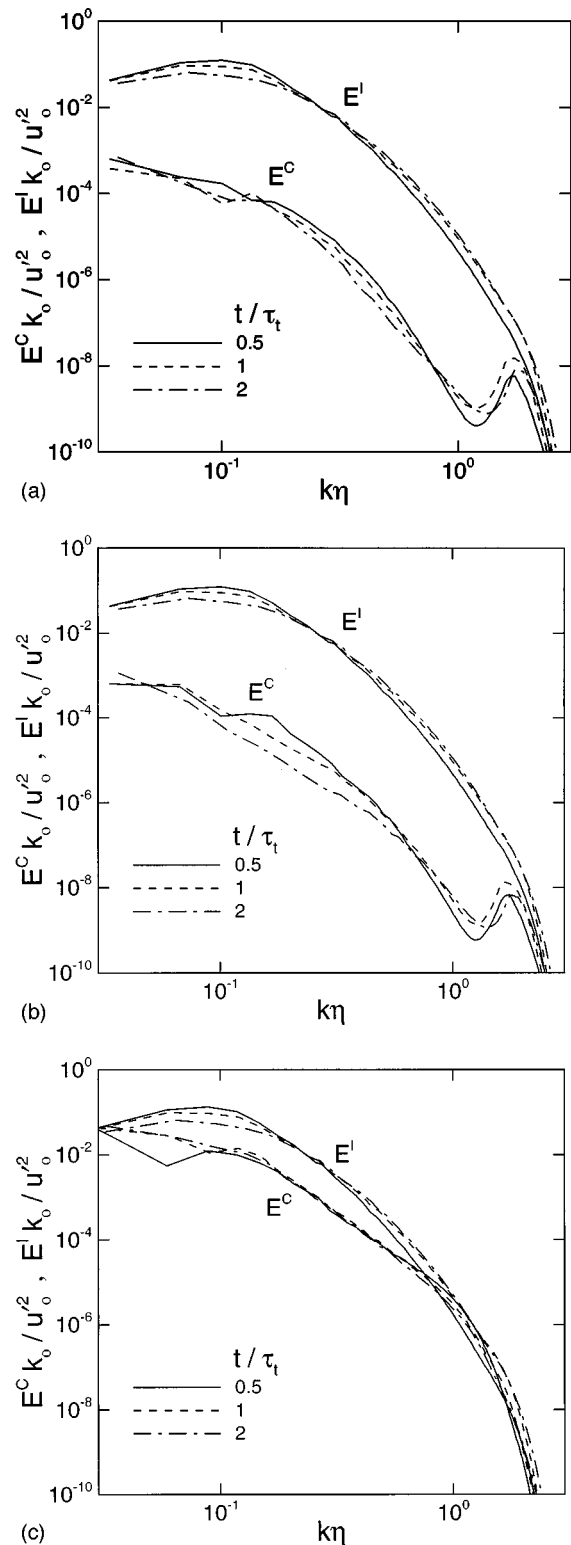

FIG. 3. Three-dimensional incompressible, E^I, and compressible, E^C, shell-averaged energy spectra for (a) nonreacting; (b) endothermic ($\overline{\Delta h^\circ} = -1$); and (c) exothermic ($\overline{\Delta h^\circ} = 2$) simulations for Da$=1$, $M_t = 0.346$, and Re$_\lambda = 34.5$.

increase in compressible energy spectrum at large wavenumber (small scales) is due to aliasing errors. (However, the level of error is small.) As time evolves, the compressible energy spectrum decays slightly at all scales, whereas the
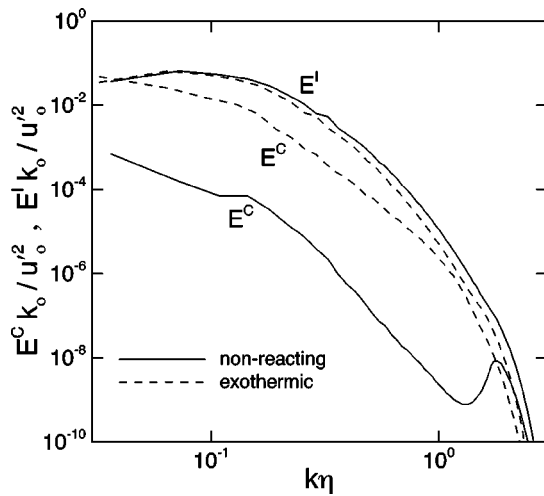
FIG. 4. Three-dimensional incompressible, E^I, and compressible, E^C, shell-averaged energy spectra for nonreacting and exothermic ($\overline{\Delta h^\circ}=2$) simulations for Da$=1$, $M_t=0.346$, and Re$_\lambda=34.5$ at $t/\tau_t=1.5$.

FIG. 5. Time evolution of rms temperature fluctuations showing the effect of $\overline{\Delta h^\circ}$ for Da$=1$, $M_t=0.346$, and Re$_\lambda=34.5$.

incompressible modes decrease at the large scales, and increase at the small scales.

Figure 3(b) plots the energy spectra for the endothermic simulation. The compressible modes are still two orders of magnitude below the incompressible modes. As time evolves, they decrease further over all except the largest scales. Figure 3(c) plots the energy spectra for $\overline{\Delta h^\circ}=2$. At all scales, the energy in the compressible modes is about two orders of magnitude higher in this case than in the nonreacting case, even surpassing the incompressible modes at the largest and smallest scales. We see that the compressible modes become more energetic as $\overline{\Delta h^\circ}$ is increased, but the incompressible modes are essentially unaffected by the level of heat release. This is shown in Fig. 4, which plots the energy spectra at $t/\tau_t=1.5$ for the non-reacting simulation and the case with the highest heat release. The incompressible energy spectra are nearly identical. It is also interesting to note that the compressible energy spectrum is increased by the same factor at all scales (except at small scales where the aliasing error is important). This is consistent with the argument that because reactions are inherently a molecular-scale process, they must be scale independent.[23]

In Fig. 5, we observe a large increase in the rms magnitude of the temperature fluctuations when the heat release is increased. Recall that from (9), a positive temperature fluctuation causes an exponential increase in the reaction rate. If the reaction is exothermic, heat is released and the local temperature increases. This further increases the temperature fluctuations, and the process feeds upon itself. However, because there is turbulent motion, the heated fluid may move to a different location before the reaction progresses further, reducing or eliminating the feedback process. Thus, the interaction between the chemical heat release and the turbulent motion should depend on the amount of heat released, $\overline{\Delta h^\circ}$, and the rate at which it is released, Da. Note that as the reaction progresses toward completion, the rate of formation of the products decreases. Therefore, the net rate of heat release decreases as well, and there is less energy to drive the
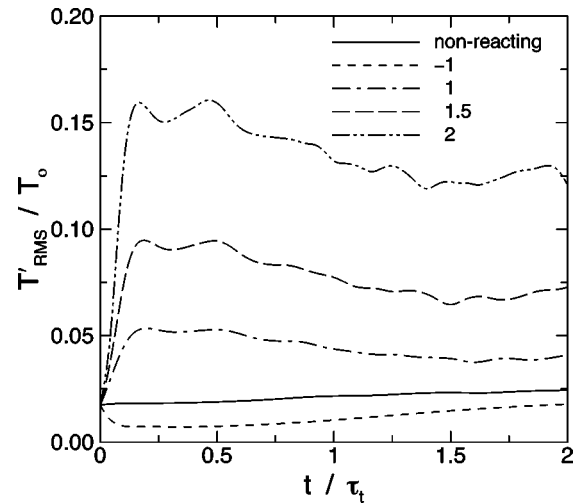
fluctuations, causing them to decrease in time. The opposite occurs for the endothermic case: $T'_{\rm rms}$ decreases initially, and then increases in time as the turbulent kinetic energy decays.

B. Damköhler number

The Damköhler number is the ratio of the chemical reaction rate to the rate of turbulent motion. For larger values of Da, chemical equilibrium is reached in a shorter time, which causes more rapid heat addition or removal. To illustrate the effect of the Damköhler number, we consider a case of moderate heat release, turbulent Mach number, and Reynolds number ($\overline{\Delta h^\circ}=1$, $M_t=0.346$, and Re$_\lambda=34.5$). Note that the total amount of energy added to the flow is the same for all simulations.

Consider Fig. 6(a), which shows the temporal evolution of the average mass fraction of the reactant species. We observe that as Da is increased, the reactants approach equilibrium at earlier times. Figure 6(b) plots the evolution of the turbulent kinetic energy. Early in the simulations, the turbulent motion is enhanced with increased Da. Accordingly, the relative compressible kinetic energy of the flow increases with increased Da. As before, the compressible energy spectrum also becomes more energetic, whereas the incompressible spectra are nearly identical for all simulations. Figure 6(c) illustrates that increased Da also increases the rms temperature fluctuations. This occurs because larger reaction rates cause the heat released to remain confined to a smaller volume of fluid, enhancing the subsequent effect on the turbulence. Thus, the localization of the heat release is important in maintaining the feedback process.

C. Turbulent Mach number

To describe the effect of the turbulent Mach number, we choose a case of moderate Damköhler number, relative heat release, and Reynolds number (Da$=1$, $\overline{\Delta h^\circ}=1$, and Re$_\lambda=34.5$). For all cases, increasing the initial Mach number causes higher values of $\langle T \rangle$ since the higher turbulent kinetic energy is dissipated and converted into internal energy. In
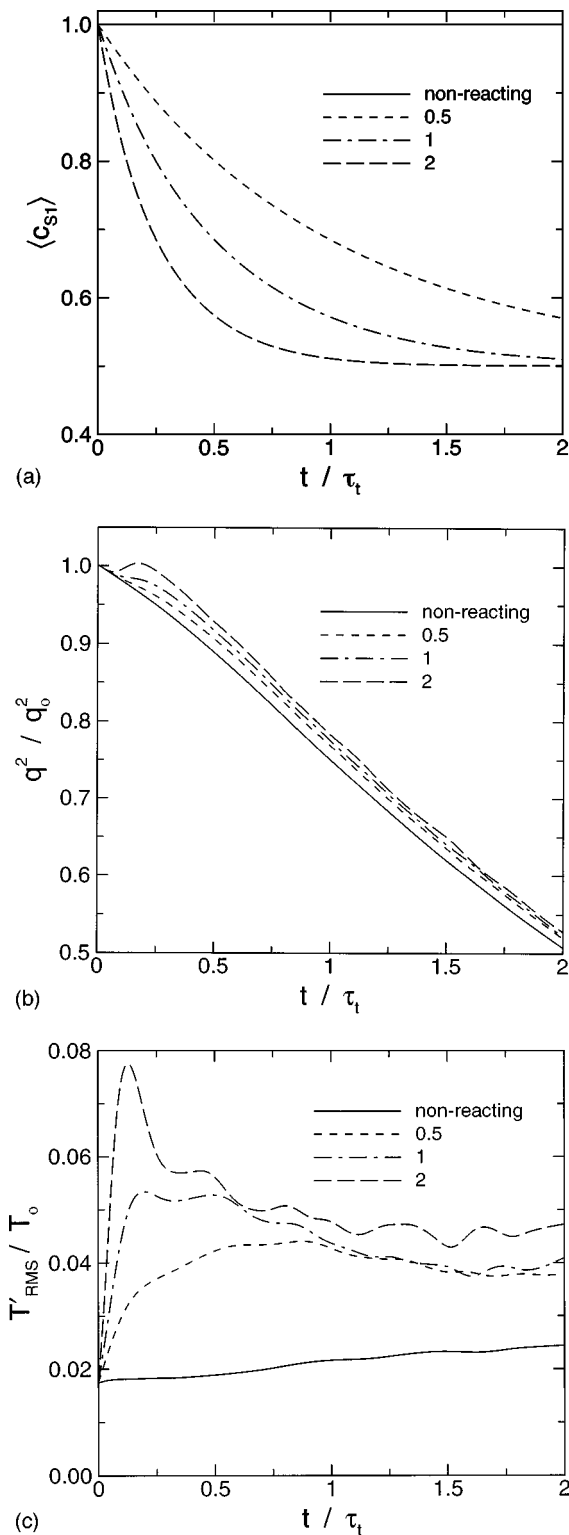
FIG. 7. Time evolution of the rms temperature fluctuations showing the effect of M_t for $\overline{\Delta h^\circ} = 1$, Da=1, and Re$_\lambda$=34.5.

fluctuations, T'_{rms}, for the case with $\overline{\Delta h^\circ} = 1$. This plot shows that the level of the temperature fluctuations is proportional to M_t^2; this is also the case in the nonreacting flows. However, relative to the nonreacting flow, the heat release increases T'_{rms} by about a factor of 2 for all M_t. Thus, the heat release amplifies the kinetic energy fluctuations, resulting in higher temperature fluctuations.

D. Reynolds number

From the direct numerical simulations we conclude that there is very little effect on the decay of reacting turbulence due to initial Reynolds numbers over the narrow range tested ($25 \leqslant$ Re$_\lambda \leqslant 50$). We observe no variation in the rate of reaction. At higher Reynolds numbers the dissipation rate is reduced, and therefore, the temperature increases more slowly and the rms temperature fluctuations are somewhat larger. However, these effects are insignificant compared to the variation of the other parameters.

VII. INTERACTION AND FEEDBACK MECHANISM

The effects of the parameters that govern the interaction between the turbulent motion and the chemical reactions have been described in the previous section. We find that the magnitude of the temperature fluctuations increases dramatically with either increased exothermicity or increased rate of reaction. The incompressible energy modes are virtually unaffected by the chemical reactions, whereas the compressible modes are strongly enhanced. The levels of compressibility increase with increased exothermicity and with increased reaction rate. From these results we can conclude that there is a feedback mechanism between the turbulent motion and the chemical reactions.

The velocity decomposition (14) is unique, and the vorticity is only a function of the incompressible velocity component. Thus, if the chemical reactions affect the incompressible component of velocity, the vorticity would also be

FIG. 6. Time evolution of (a) average mass fraction of reactants; (b) turbulent kinetic energy; and (c) rms temperature fluctuations showing the effect of Da for $\overline{\Delta h^\circ} = 1$, M_t=0.346, and Re$_\lambda$=34.5.

the non-reacting simulations, the relative turbulent kinetic energy, q^2/q_o^2, decay rate depends weakly on the initial M_t. For the exothermic simulations, the turbulent kinetic energy increases initially. This increase is proportional to the initial M_t.

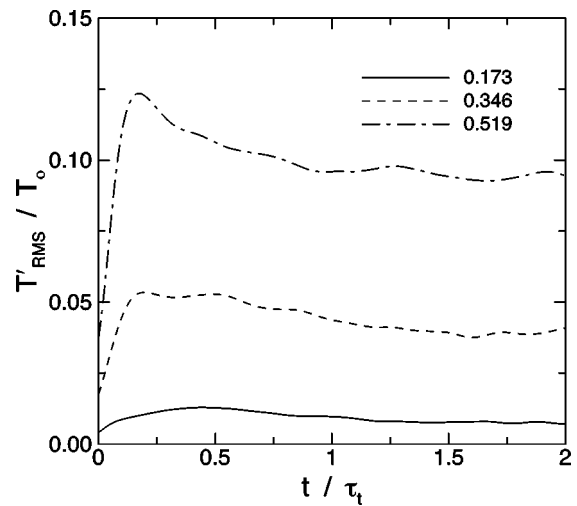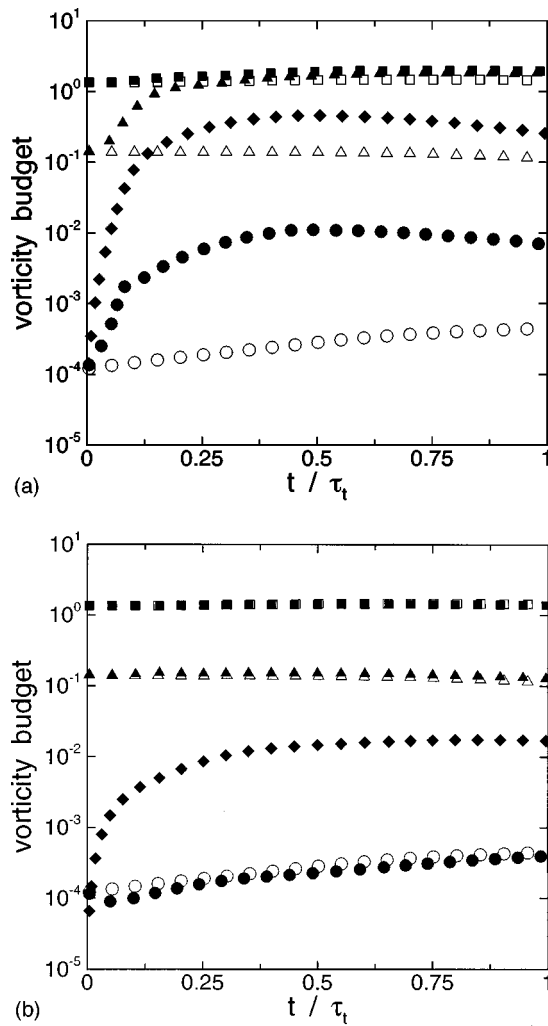Figure 7 plots the temporal evolution of rms temperature

FIG. 9. Time evolution of vorticity magnitude showing the effect of $\overline{\Delta h^\circ}$ for $M_t = 0.346$, $Re_\lambda = 34.5$, and Da=1.

FIG. 8. Normalized vorticity, $|\boldsymbol{\omega}_t| \tau_t/\omega_o$, budget for nonreacting (empty symbols) and (a) exothermic ($\overline{\Delta h^\circ} = 2$) (filled symbols); and (b) endothermic ($\overline{\Delta h^\circ} = -1$) (filled symbols) simulations for Da=1, $M_t = 0.346$, and $Re_\lambda = 34.5$; ($\square$), stretching production; ($\triangle$), compressible destruction; ($\bigcirc$), nonreacting entropy production; ($\diamondsuit$), reacting entropy production.

affected. Therefore, let us consider the evolution of the vorticity during the simulations. We can write the total change of vorticity as

$$\frac{D\boldsymbol{\omega}}{Dt} = (\boldsymbol{\omega} \cdot \nabla)\mathbf{u} - \boldsymbol{\omega}(\nabla \cdot \mathbf{u}) + \nabla T \times \nabla S, \qquad (18)$$

where S is the entropy and we have neglected the diffusive terms. These terms represent the production of vorticity due to vortex line stretching, compressibility, and thermodynamic changes, respectively. We can decompose the third term by noting that for a mixture of thermally perfect gases

$$S = c_p \ln T - R \ln p + \sum_s c_s \frac{h_s^\circ - \mu_s^\circ}{T}, \qquad (19)$$

where c_p is the specific heat at constant pressure of the gas mixture, R is the gas constant, and μ_s° is the chemical potential of species s. The first two terms form part of the entropy even when the gas is not chemically reacting, and the third term is the entropy due to chemical reactions. Thus, we can
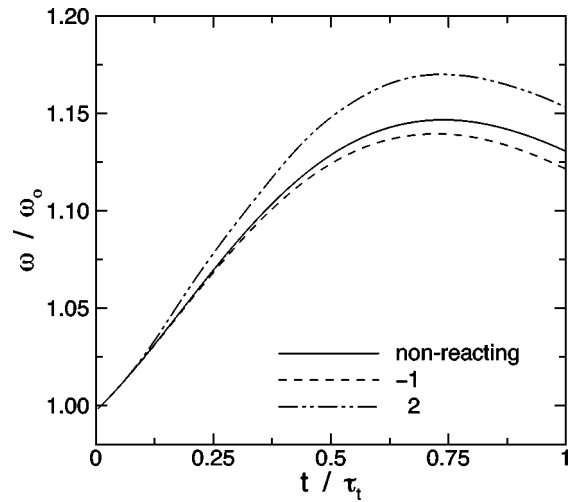
separate the production of vorticity due to thermodynamic changes into two components, and refer to them as the nonreacting entropy and the reacting entropy. Note that had we used a more complicated reaction, it would be more difficult to make this decomposition because the mixture c_p and R would also change.

Figure 8(a) plots the budget of vorticity for a nonreacting simulation and an exothermic simulation with $\overline{\Delta h^\circ} = 2$. There is a large difference in the order of magnitude between the terms. The main contribution to vorticity production is due to the vortex stretching and turning term for both simulations. Whereas the compressibility term remains nearly unchanged for the non-reacting case, it reaches the same order of magnitude as the stretching term for the exothermic simulation. The thermodynamic effects due to the nonreacting entropy are larger for the exothermic simulation, although they are three orders of magnitude below the terms mentioned above. The thermodynamic contribution due to the reacting entropy is initially zero for the exothermic simulation, but increases to a value that is about an order of magnitude lower than the stretching and compressible terms. Thus, the main contributions to the vorticity budget are the vortex line stretching and turning and compressibility effects.

Figure 8(b) illustrates the same vorticity budget for the nonreacting simulation and an endothermic case with $\overline{\Delta h^\circ} = -1$. Again, the main contribution to vorticity production is from the vortex line stretching and turning term. For the endothermic simulation, the compressible destruction increases and the reacting entropy production is nonzero, but small.

Figure 9 plots the temporal evolution of the average vorticity magnitude for the nonreacting case and two reacting cases. We see that the vorticity magnitude does not vary appreciably with increasing heat release. This occurs because the heat released by the chemical reactions does not produce vorticity by itself. Rather, the reactions affect the turbulence locally, enhancing compressions and expansions, which redistribute the vorticity, concentrating or diluting it. In flows
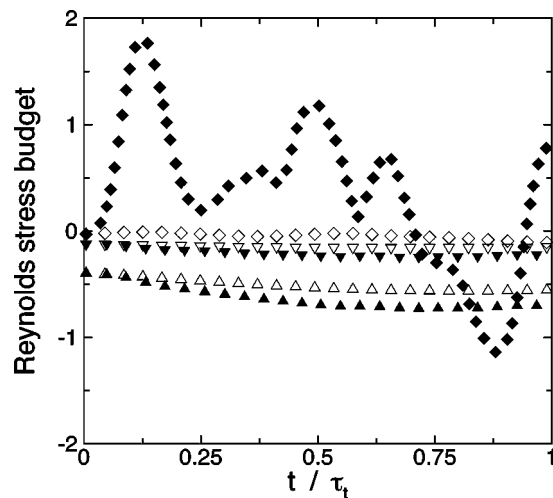
FIG. 10. Normalized Reynolds stress, $R_{22,t}/\epsilon_\circ$, budget for nonreacting (empty symbols) and exothermic (filled symbols) simulations for $M_t = 0.346$, $Re_\lambda = 34.5$, $Da = 1$, and $\overline{\Delta h^\circ} = 2$; ($\diamond$), pressure-strain; ($\nabla$), viscous diffusion; ($\triangle$), dissipation.

with turbulence-induced shock waves, the thermodynamic generation of entropy can be a major contributor to the generation of vorticity through baroclinic torques.[24] However, in the simulations considered here, there are no significant shock waves, and the entropy is generated with no directional preference. Therefore, the baroclinic torques do not contribute to the average vorticity. (It should be noted that this conclusion depends on how the turbulence is initialized. If the approach of Blaisdell and Ristorcelli is not used, shock waves will be present and the baroclinic torques can be important.) Another source of vorticity is due to the chemical potential in (19). This term also does not contribute to vorticity generation because the mass fraction gradients are closely aligned with the temperature gradients in the flows under consideration; this observation was also made by Greenberg.[25]

The results also corroborate the theoretical work of Eschenroeder,[26] who found that the turbulent motion is fed from the external energy source provided by the chemical reactions. Our results show that the chemical energy produces local high temperature and pressure regions, which then produce increased kinetic energy through the reversible work term, $p\nabla \cdot \mathbf{u}$, in the kinetic energy equation. We can see the effect of this process on the Reynolds stress by considering the Reynolds stress budget

$$R_{ij,t} = -(Q_{i,j} + Q_{j,i}) + \nu R_{ij,kk} - T_{ijk,k} - \nu\epsilon_{ij} + \Pi_{ij}. \quad (20)$$

Where $R_{ij} = \overline{u_i u_j}$ is the Reynolds stress tensor, $Q_i = \overline{p u_i/\rho}$ is the pressure–velocity correlation, $T_{ijk} = \overline{u_i u_j u_k}$ is the triple velocity correlation tensor, $\epsilon_{ij} = 2\overline{u_{i,k} u_{j,k}}$ is the homogeneous dissipation rate tensor, and $\Pi_{ij} = \overline{p(u_{i,j} + u_{j,i})/\rho}$ is the pressure-strain term. The pressure transport and the turbulent transport are statistically zero. Figure 10 shows the budget of the $R_{22,t}$ component for the nonreacting and exothermic simulations. The pressure-strain term is nearly zero in the nonreacting case, but it is the dominant term in the exothermic simulation. Note that in this case, there are oscillations

in the pressure–strain production term, whose nondimensional period is approximately equal to the local Mach number. This indicates that these oscillations are a result of acoustic (pressure) waves. This further illustrates that the Reynolds stress generation is mainly caused by compressibility effects in the reacting case.

VIII. CONCLUSION

In this paper we investigate the interaction of isotropic turbulence and a chemical reaction at conditions typical of a hypersonic boundary layer. We use a modified reaction rate that preserves the important features of the Arrhenius rate expression, and makes it possible to perform a systematic analysis. The flow is parametrized by four nondimensional numbers: the turbulent Mach number, Reynolds number, relative heat release, and relative reaction rate.

The direct numerical simulations show that the heat released by an exothermic reaction produces regions of high temperature and pressure. This causes localized expansions which increase the compressible turbulent kinetic energy. This results in increased rates of kinetic energy decay, vorticity production, and Reynolds stress production. Simultaneously, in regions of high temperature the reaction rate increases, further increasing the heat release and the temperature. Thus, there is a positive feedback between the chemical reactions and the turbulent motion. The strength of the feedback process depends on the amount of heat released, the reaction rate, and more weakly on the turbulent Mach number. When the reaction is endothermic, the feedback is negative and temperature fluctuations are damped.

[1] I. Glassman, *Combustion,* 3rd ed. (Academic, New York, 1996), Chap. 4.

[2] A. D. Leonard and J. C. Hill, ''Direct numerical simulation of turbulent flows with chemical reaction,'' J. Sci. Comput. **3**, 25 (1988).

[3] A. Picart, R. Borghi, and J. P. Chollet, ''Numerical simulation of turbulent reactive flows,'' Comput. Fluids **16**, 475 (1988).

[4] W. H. Jou and J. J. Riley, ''Progress in direct numerical simulations of turbulent reacting flows,'' AIAA J. **27**, 1543 (1989).

[5] P. A. McMurtry, J. J. Riley, and R. W. Metcalfe, ''Effects of heat release on the large-scale structure in turbulent mixing layers,'' J. Fluid Mech. **199**, 297 (1989).

[6] F. Gao and E. E. O'Brien, ''Direct numerical simulation of reacting flows in homogeneous turbulence,'' AIChE. J. **37**, 1459 (1991).

[7] P. Givi, C. K. Madnia, C. J. Steinberger, M. H. Carpenter, and J. P. Drummond, ''Effects of compressibility and heat release in a high speed reacting mixing layer,'' Combust. Sci. Technol. **78**, 33 (1991).

[8] F. F. Grinstein and K. Kailasanath, ''Chemical energy release and dynamics of transitional, reactive shear flows,'' Phys. Fluids A **4**, 2207 (1992).

[9]C. J. Montgomery, G. Kosály, and J. J. Riley, ''Direct numerical simulation of turbulent reacting flow using a reduced hydrogen-oxygen mechanism,'' Combust. Flame **95**, 247 (1993).

[10]R. S. Miller, K. Madnia, and P. Givi, ''Structure of a turbulent reacting mixing layer,'' Combust. Sci. Technol. **99**, 1 (1994).

[11]Y. Y. Lee and S. B. Pope, ''Nonpremixed turbulent reacting flow near extinction,'' Combust. Flame **101**, 501 (1995).

[12]N. Swaminathan, S. Mahalingam, and R. M. Kerr, ''Structure of nonpremixed reaction zones in numerical isotropic turbulence,'' Theor. Comput. Fluid Dyn. **8**, 201 (1996).

[13]C. J. Montgomery, G. Kosály, and J. J. Riley, ''Direct numerical simulation of turbulent reacting flow using a reduced hydrogen-oxygen mechanism,'' Combust. Flame **109**, 113 (1997).

[14]F. A. Javery, R. S. Miller, F. Mashayek, and P. Givi, ''Differential diffusion in binary scalar mixing and reaction,'' Combust. Flame **109**, 561 (1997).

[15]R. N. Gupta, J. M. Yos, R. A. Thompson, and K. Lee, ''A review of reaction rates and thermodynamic and transport properties for an 11-species air model for chemical and thermal non-equilibrium calculations to 30,000 K,'' NASA RP-1260 (1990).

[16]S. Lee, S. K. Lele, and P. Moin, ''Eddy-shocklets in decaying compressible turbulence,'' Phys. Fluids **3**, 657 (1991).

[17]W. C. Reynolds, ''The potential and limitations of direct and large eddy simulations,'' Lect. Notes Phys. **357**, 313 (1991).

[18]J. R. Ristorcelli and G. A. Blaisdell, ''Consistent initial conditions for the DNS of compressible turbulence,'' Phys. Fluids **9**, 4 (1997).

[19]G. A. Blaisdell and J. R. Ristorcelli, ''Consistent initial conditions for the DNS of compressible turbulence,'' APS Division of Fluid Dynamics Meeting (1996).

[20]S. Tavoularis, J. C. Bennett, and S. Corrsin, ''Velocity derivative skewness in small Reynolds number nearly isotropic turbulence,'' J. Fluid Mech. **88**, 63 (1978).

[21]S. A. Orszag and J. S. Patterson, ''Numerical simulation of three-dimensional homogeneous isotropic turbulence,'' Phys. Rev. Lett. **28**, 76 (1972).

[22]J. E. Moyal, ''The spectra of turbulence in a compressible fluid; eddy turbulence and random noise,'' Proc. Cambridge Philos. Soc. **48**, 329 (1951).

[23]P. Moin, ''Progress in large eddy simulation of turbulent flows,'' AIAA Paper No. 97-0749 (1997).

[24]T. Passot and A. Pouquet, ''Numerical simulation of compressible homogeneous flows in the turbulence regime,'' J. Fluid Mech. **181**, 441 (1987).

[25]R. A. Greenberg, ''Non-equilibrium vortex flow in a dissociating gas,'' J. Aerosp. Sci. **29**, 1484 (1962).

[26]A. Q. Eschenroeder, ''Intensification of turbulence by chemical heat release,'' Phys. Fluids **7**, 1735 (1964).